CAL Project No. AN-2112-Y

CORNELL AERONAUTICAL LABORATORY, INC.
Buffalo, New York 14221

Quarterly Progress Report No. 5

SHOCK TUNNEL INVESTIGATIONS OF TURBULENT FLOW AT HIGH MACH NUMBERS

Contract No. NSR 33-009-029
Project No. PR 10-6222

Reporting Period: 1 July 1966 through 30 September 1966

Objective

The objective of this investigation is to further develop instrumentation for shock tunnel studies of turbulent boundary layers and to obtain preliminary experimental information in the boundary layer of the hypersonic shock tunnel nozzle.

Nozzle Wall Boundary Layer Profiles

Attention has been given during this reporting period to the interpretation of nozzle wall boundary layer pitot pressures obtained from the two-foot exit diameter contoured "A" nozzle of the CAL Hypersonic Shock Tunnel. These efforts were limited by the apparent unreliability of the type of pitot probe used in the outer boundary layer and by the lack of a direct measurement of the total enthalpy in the boundary layer. Nevertheless, approximately the lower third of the boundary layer was covered by the more reliable pitot probes in addition to the measured static pressure at the wall. The unit Prandtl number Crocco relation $\frac{u}{u_\delta} = \frac{H - h_w}{H_\delta - h_w}$ was used in the absence of a direct enthalpy measurement. The implied boundary layer assumptions will be examined later. In turbulent boundary layer profile experiments performed at NOL, in which both pitot pressure and total temperature measurements were obtained on both a cooled, two-dimensional contoured nozzle wall (Ref. 1) and on a cooled

sharp flat plate in the test section of the same nozzle (Refs. 2 and 3), it was observed that departures from the Crocco relation occurred near the wall. For the NOL data, in the nozzle case, the total temperatures lie above the Crocco relation near the wall, whereas for the flat plate the reverse is true. (The departure is more extreme in the data of Hill, Refs. 4 and 5, which were obtained in nitrogen flow through a small, conical nozzle.) Other investigators have reacted in diverse ways to these observations. In comparison with a modified Crocco relation, which replaces the local total enthalpy with the recovery enthalpy in the boundary layer, Walz (Ref. 6) examines the above experimental observations and concludes that, because of the disagreement, the experiments must be wrong. Rotta (Refs. 7, 8 and 9) examines the same results and concludes that the Crocco relation is invalid for high ratio of heat transfer to the wall. It should be noted here that numerous investigators, for example, Baronti and Libby (Ref. 10) have observed good agreement between the Crocco relation and adiabatic wall experimental data. Baronti and Libby (Ref. 10), in applying the law of corresponding stations of Coles (Ref. 11 extended by Crocco. Ref. 12) to a rigorous point-by-point mapping of the boundary layer profile, find that for boundary layer integrals and evaluation of the static temperature in the boundary layer, the unit Prandtl number form of the Crocco relation is satisfactory for all but Hill's conical nozzle data, where it was necessary to use the experimentally determined temperatures.

Thus, although some question exists concerning the validity of the Crocco relation in the present case, it has been used in the absence of either a better theoretical approach or a direct measurement to enable some evaluation of the data in hand. The pitot pressure data from the boundary layer probes adjacent to the wall were used to establish the inner portion of the profiles. Pressures indicated by the type of probe used in the outer boundary layer tended to fall well above either the wall probe pressures or conventional freestream pitot probe pressures where overlapping measurements were made. However, because the profile so obtained was in qualitative agrument with estimates based on a $1/9^{th}$ power law velocity profile and the Crocco relation (see figure 1), these outer layer probe values

were used to aid extrapolations to the boundary layer edge. The edge pitot pressures were computed from pitot survey rake averages at comparable test conditions. These values were generally within 5 percent of test values in a probe near the nozzle axis. Velocity and density profiles were computed from the measured pitot profiles and the assumed Crocco relation in accordance with the approach outlined in Quarterly Progress Report No. 2: a Mach number profile is obtained from the pitot pressure profile assuming static pressure constant through the boundary layer, the velocity profile follows from the energy equation and the Crocco relation, static enthalpy and density follow from the energy equation and equation of state, respectively. The resulting Mach number and velocity profiles are shown in Figures 2 and 3, respectively. Data from repeat runs were combined as shown in Table I. Table I tabulates edge conditions based both on a measured wall static pressure and on average survoy rate pitot pressure obtained in calibration runs.

In constant density flows the velocity profile has been found to be characterized by two similarity laws, the law of the wall for the inner region close to the wall and the velocity defect law (also law of the wake or momentum-defect law) in the outer portion of the boundary layer (both summarized in Ref. 13). These similarity laws are written

$$\frac{u}{u_\tau} = f\left(y\frac{u_\tau}{\nu_w}\right)$$

$$= y\frac{u_\tau}{\nu_w} \qquad \text{for the laminar sublayer}$$

$$= A\ell n\left(y\frac{u_\tau}{\nu_w}\right) + B \qquad \text{for the remainder of the wall region}$$

and

$$\frac{u-u_e}{u_\tau} = F\left(\frac{y}{\delta}\right) \qquad \text{in the velocity defect region}$$

$$= A\ell n\ \frac{y}{\delta} - A\pi(x)\left[2-W\left(\frac{y}{\delta}\right)\right] \text{ (after Coles, Ref. 11)}$$

where u_τ is the friction velocity, $\sqrt{\frac{\tau_w}{\rho_w}}$.

Several efforts have been made to relate the compressible velocity profiles (with wall heat transfer) to these incompressible, constant density laws. Baronti and Libby (Ref. 10) have shown that the NOL and velocity profile data (Refs. 1-3) can be made to correlate satisfactorily and to transform to the constant density profiles for a selected value of skin friction coefficient. However, the approach of Ref. 10 is a rather tedious, trial-and-error procedure and has not been attempted here.

In earlier work, Deissler and Loeffler (Ref. 14) at NASA Lewis developed predictions of the velocity profiles for the compressible turbulent boundary layer with heat transfer by assuming relations for the eddy diffusivities and the ratios of heat transfer and skin friction to values at the wall and integrating the resulting energy and momentum equations. Their results are presented in terms of $\frac{u}{u_\tau}$ as a function of $y \frac{u_\tau}{\nu_w}$ and of the wall shear and heat transfer. The present nozzle boundary layer data have been plotted in terms of $\frac{u}{u_\tau}$ as a function of $y \frac{u_\tau}{\nu_w}$, using the measured wall shear in calculating u_τ. These are presented in Figure 4 and compared with the NOL nozzle and flat plate data and with the predictions of Ref. 14. In the region near the wall it can be seen that there is some correlation between the present velocity profile data and the NOL data. This correlation is expected in view of the relatively small effect of heat transfer on the velocity profile near the wall predicted by Ref. 14. Farther from the wall, the prediction of Ref. 14, although disagreeing in magnitude, agrees with the trend of the present velocity data and predicts approximately the observed effect of wall heat transfer on the velocity profile as noted in the difference between the data for $\frac{(T_{A_w} - T_w)}{T_{A_w}} = 0.7$ and those for $\frac{(T_{A_w} - T_w)}{T_{A_w}} = 0.9$.

Since wall values would not be expected to be primary parameters in the outer portion of a compressible boundary layer with wall heat transfer, a correlation of the defect portion of the boundary layer has been made in terms of

$$\frac{u_e - u}{v^*} \text{ vs. } \frac{y}{\delta}$$

where v^* is a friction velocity based on local density,

$$v^* = \sqrt{\frac{\tau_w}{\rho}} \quad .$$

The results are compared in Figure 5 with typical values for the constant density case with typical values of the pressure gradient parameter, π. The data correlate and, with density evaluated locally, are in reasonable agreement with the defect prediction.

Using the computed velocity and density profiles, integrations have been performed to obtain the displacement thickness, δ^*, and the momentum defect thickness, θ, which are expressed for the axially symmetric nozzle case as

$$\frac{\delta^*}{\delta}\left(\frac{2r_w}{\delta} - \frac{\delta^*}{\delta}\right) = \int_{\frac{r_w}{\delta}-1}^{\frac{r_w}{\delta}} \frac{2r}{\delta}\left(1 - \frac{\rho u}{\rho_e u_e}\right) d\frac{r}{\delta}$$

and

$$\frac{\theta}{\delta}\left(\frac{2r_w}{\delta} - \frac{\theta}{\delta}\right) = \int_{\frac{r_w}{\delta}-1}^{\frac{r_w}{\delta}} \frac{2r}{\delta}\,\frac{\rho u}{\rho_e u_e}\left(1 - \frac{u}{u_e}\right) d\frac{r}{\delta}$$

where r is the radial distance from the nozzle centerline and r_w locates the nozzle wall, or in terms of a coordinate, y, normal to the wall

$$\frac{\delta^*}{\delta} - \frac{\delta}{2r_w}\left(\frac{\delta^*}{\delta}\right)^2 = \int_0^1 \left(1 - \frac{\rho u}{\rho_e u_e}\right)\left(1 - \frac{y}{r_w}\right) d\frac{y}{\delta}$$

$$\frac{\theta}{\delta} - \frac{\delta}{2r_w}\left(\frac{\theta}{\delta}\right)^2 = \int_0^1 \frac{\rho u}{\rho_e u_e}\left(1 - \frac{u}{u_e}\right)\left(1 - \frac{y}{r_w}\right) d\frac{y}{\delta}$$

These expressions collapse to the familiar two-dimensional forms when $\delta << r_w$. However, in the present cases, for which the maximum boundary layer thickness was 2.73 inches in a nozzle of 12-inch radius, the difference between the axially symmetric case and the two-dimensional case was found to be at most, five percent. The tabulated values are from the axially symmetric form.

Nozzle Wall Measurements of Skin Friction and Heat Transfer

The nozzle wall data have been compared with theory using the local Reynolds number based on momentum thickness and based on flow length from the nozzle throat. Edge conditions have been computed in turn, for equilibrium expansion to the measured wall pressure at the profile station and to the average survey rake pitot pressure obtained in calibration runs. Both results are shown on the figures. Theory values were computed from the edge conditions based on wall static pressure in Table I. Comparisons will also be made with values from Table I using calibration pitot pressures and any significant differences noted in the future. The measured skin friction and wall heat transfer values are compared in Figures 6 and 7, respectively, with several predictions:

1. Blasius, reference enthalpy (Ref. 15) - The constant density form

$$C_f = \frac{0.0176}{(Re_\theta)^{0.2}}$$

is used with the density and viscosity evaluated at a mean boundary layer enthalpy computed by substituting the Crocco relation in $h_* = \int h d\frac{u}{u_\delta}$ or

$$h_{*\,mean} = 0.5 h_w + 0.333 h_\delta + 0.1667 H_{A_w}$$

Note that the Eckert reference enthalpy is practically equivalent,

$$h_{*\,Eckert} = 0.5 h_w + 0.28 h_\delta + 0.22 H_{A_w}$$

2. Karman - Schoenherr, reference enthalpy (Ref. 15) - The logarithmic constant density form

$$C_f = \frac{0.0586}{(\log 2Re_\theta)\left[\log 2Re_\theta + 0.868\right]}$$

is again evaluated at a mean reference enthalpy.

3. Walz (Ref. 6) - The theory of Walz is computed using both his theoretical expressions for profile integral parameters and the experimentally determined ones

$$C_f \equiv \frac{\tau_w}{\frac{1}{2}\rho u_\delta} = \frac{\alpha(H_{12})}{R_{\delta_2}^{0.268}} \quad \frac{\delta 2}{\delta_2)_u}$$

where

$$\alpha(H_{12}) = (0.246)10^{-0.678 H_{12}}$$

$$H_{12} = \left(\frac{\delta_1}{\delta_2}\right)_u$$

$$\delta_1)_u = \int_0^1 \left(1 - \frac{u}{u_\delta}\right) d\left(\frac{y}{\delta}\right)$$

$$\delta_2)_u = \int_0^1 \frac{u}{u_\delta}\left(1 - \frac{u}{u_\delta}\right) d\left(\frac{y}{\delta}\right)$$

$$R_{\delta_2} = \frac{\rho_\delta u_\delta \delta_2}{\mu_w}$$

$$\delta_2 = \theta = \int_0^1 \frac{\rho u}{\rho_\delta u_\delta}\left(1 - \frac{u}{u_\delta}\right) d\left(\frac{y}{\delta}\right)$$

4. Spalding and Chi (Ref. 16) - The semi-empirical theory of Spalding and Chi assumes that compressible boundary layer skin friction can be transformed to incompressible form

$$F_c\, C_f = \phi\left(F_{R_\theta}\, R_\theta\right)$$

with

$$F_c = f_1\left(M_\delta, \frac{T_\delta}{T_w}\right)$$

$$F_{R_\theta} = f_2\left(M_\delta, \frac{T_\delta}{T_w}\right)$$

Values have been computed using the local conditions for the nozzle boundary layers and the momentum thickness, θ, from the integration of the experimental boundary layer profiles.

5. Winkler and Cha (Refs. 2 and 3) - A purely empirical evaluation of temperature ratio effects in compressible boundary layers with heat transfer was made by Winkler and Cha with the result that the data they evaluated were best correlated by

$$\left(\frac{T_o}{T_\infty}\right)^{1/2}\left(\frac{T_{Aw}}{T_w}\right)^{1/4} C_f = 0.0246\, Re_\theta^{-0.251}$$

The results for skin friction are shown in Figure 6, compared with the experimental data. The reference enthalpy and Walz (experimental profiles) approaches generally over-predict the skin friction -- by over 100 percent in one case -- whereas the Winkler-Cha correlation formula and the theoretical Walz expression fall far below the present data. It is noteworthy that in the data correlated by the Winkler and Cha formula, wall temperature ratios are at most $\frac{T_{Aw}}{T_w} = 2$ whereas in the present case, $\frac{T_{Aw}}{T_w}$ ranges from 3 to 10. Thus, the factor $\left(\frac{T_{Aw}}{T_w}\right)^{1/4}$ is as large as 1.78 in the present case compared with a maximum of 1.19 in Ref. 3. Data normalized with edge conditions calculated from calibration pitot pressures provide the most consistent agreement with the Spalding-Chi prediction.

A much smaller exponent could also correlate the present data without destroying the correlation of data shown in Ref. 3. In fact, it appears that if this exponent were set equal to zero, both the present data and those of Ref. 3 would correlate to within ±20 percent. The semi-empirical theory of Spalding and Chi, however, has already been found to correlate numerous data points for which a direct measurement of skin friction was made and is seen to provide the most consistent agreement with present data of all the theories and methods examined.

In comparing the heat transfer data with the same theories and methods as for the skin friction data, the most commonly employed modified Reynolds analogy, the relationship developed by Colburn, has been used, viz.,

$$St = \frac{C_f}{2 P_r^{2/3}}$$

It was observed in the previous progress report in examining the nozzle wall data that this relationship tends to overestimate the observed ratio between heat transfer and skin friction. However, it is a straightforward, well-defined relationship and suffices for present purposes, pending further examination of the Reynolds analogy prediction later in this report. The heat transfer data are presented in terms of the Stanton number as a function of the local momentum thickness Reynolds number in Figure 7. The consistency of the experimentally observed ratio between Stanton number and skin friction coefficient is such that essentially the same comparisons with theory are seen as for skin friction, although the Colburn relation shifts the theories upward relative to the heat transfer data.

Again it is noted that without any modification, the Spalding-Chi prediction provides most consistent agreement with the data, whereas if the $\frac{T_{Aw}}{T_w}$ dependence were omitted, the Winkler-Cha skin friction correlation formula would predict the Stanton number to within 20 percent.

As an addition to the comparisons of nozzle wall data with Reynolds analogy formulations reported in the previous progress letter, the modified Reynolds analogy of Cohen (Ref. 17) developed for flows with pressure gradients and Prandtl number of unity has been examined. The Cohen result can be written

$$2\,\frac{C_H}{C_f}\,\frac{H_e - H_w}{H_e} = \frac{\delta_h}{\theta} + 2\,\frac{\theta}{C_f}\,\frac{d\frac{\delta_h}{\theta}}{dx} - 2\,\frac{\delta_h}{C_f}\left(1 + \frac{\delta^*}{\theta}\right)\frac{1}{u_\delta}\,\frac{d u_\delta}{dx}$$

where the energy loss (enthalpy convection) thickness, δ_h, is

$$\delta_h = \int_0^1 \frac{\rho u}{\rho_\delta u_\delta}\left(1 - \frac{H}{H_e}\right) d\left(\frac{y}{\delta}\right)$$

When, as in the present case, the Crocco relation $\frac{u}{u_\delta} = \frac{H - H_w}{H_e - H_w}$ is assumed, the enthalpy convection and momentum defect thickness are related by $\delta_h = \left(1 - \frac{H_w}{H_e}\right)\theta$ so that the term $\frac{d\frac{\delta_h}{\theta}}{dx}$ is identically zero and the Reynolds analogy expression may be written

$$2\,\frac{C_H}{C_f} = 1 - \frac{2\theta}{C_f}\left(1 + \frac{\delta^*}{\theta}\right)\frac{1}{u_\infty}\,\frac{d u_\infty}{dx}$$

For the present data the velocity gradient in the flow direction can, in principle, be obtained from the measurement of static pressure at the wall, recorded at four stations at 6 to 10 feet from the nozzle throat, the last measurement being taken at the same station as the pitot pressure profile data. However, the wall static pressure measurements are not considered sufficiently reliable for this purpose. Furthermore, since the term with the gradient in profile parameter δ_h/θ is opposite in sign to that of the velocity gradient term, it may be deceptive to attempt to include only one of these terms. Since the effect of Prandtl numbers being less than one has been to increase $2C_H/C_f$ in the zero pressure gradient cases, as seen in the previous progress report, modification of the Cohen result to include Prandtl number as well as velocity gradient might produce reasonable agreement. This has not been attempted here, however. It will be noted that the flat plate data examined in the following section tend to show ratios of heat transfer to skin friction that are quite comparable to the nozzle measurements.

Comparison with Flat Plate Experiments

An important question pertainant to the applicability of nozzle wall boundary layer experiments is whether the upstream history is such as to create significant differences from a zero pressure gradient, flat plate turbulent boundary layer. Therefore, a comparison has been made between the nozzle results and measurements of surface heat transfer and skin friction obtained on a 15 by 24 inch, sharp leading edge flat plate as part of a related study on turbulent flows.* These experiments were performed in the contoured nozzles of the CAL Hypersonic Shock Tunnel, 96-Inch Leg. By generating high reservoir pressure conditions, model surface flow length Reynolds numbers were obtained in the same range as those obtained in the nozzle wall experiments. It should be noted that whereas a finite pressure

*Air Force Contract No. AF 33(615)-1847, administered by the Research and Technology Division (FDMG).

gradient exists along the nozzle wall, where upstream waves are being cancelled, the pressure gradient along the nozzle centerline (the model location) is negligible. Representative data from the sharp plate experiments are presented in Figures 8 and 9 in terms of the Spalding-Chi correlation parameters. The data taken with the instrumented surface at a compression angle of 10 degrees are presented in terms of local wedge conditions based on the oblique shock calculation. The nozzle data examined previously are also presented as a function of the Reynolds number based on local conditions and the flow length from the nozzle throat. The fact that the nozzle data bear the same comparison with Spalding-Chi theory in both the momentum thickness Reynolds number form (Figures 6 and 7) and the flow length Reynolds number form (Figures 8 and 9) suggests that the length of boundary layer flow in the low pressure gradient portion of the nozzle is sufficient to approach flat plate conditions. The correlation of flat plate and nozzle data in Figures 8 and 9, further support this hypothesis. Further experimentation with detailed boundary layer profile measurements is required to develop a clearer picture, but a tentative conclusion is that turbulent boundary layers typical of flat plate flows can be developed on the shock tunnel contoured nozzle wall.

Current Status and Future Plans

An advance copy of the negotiated supplemental agreement, amending this contract to extend the performance period to September 30, 1967 and increasing the authorized costs (not including fee) to $148,712, has been received.

As of 30 September 1966, funds expended on this contract were $60,117.

REFERENCES

1. Lobb, R. K., Winkler, E. M., and Persh, S.:
"Experimental Investigation of Turbulent Boundary Layers in Hypersonic Flow," Journal of Aeronautical Sciences, Vol. 22, No. 1, January 1955, pp. 1-9 (Also as NAVORD Report 3880, 1955).

2. Winkler, E. M., and Cha, M.:
"Investigation of Flat Plate Hypersonic Turbulent Boundary Layer with Heat Transfer at a Mach Number of 5.2," NAVORD Report 6631, 1959.

3. Winkler, E. M.:
"Investigation of Flat Plate Hypersonic Turbulent Boundary Layer with Heat Transfer," Transactions of the ASME, Journal of Applied Mechanics, Vol. 28, 1961 (same data)

4. Hill, F. K.:
"Boundary Layer Measurements in Hypersonic Flow," Journal of Aeronautical Sciences, Vol. 23, 1956, pp. 35-42.

5. Hill, F. K.:
"Turbulent Boundary Layer Measurements at Mach Numbers of 8 to 10," Physics of Fluids, Vol. 2, 1959, pp. 668-680.

6. Walz, A.:
"Compressible Turbulent Boundary Layers," The Mechanics of Turbulence, Science Publishers, Inc., New York, 1964 (Proceedings of Colloque Internationale sur "La Mechanique de la Turbulence," Marseille, August 28 to September 2, 1961).

7. Rotta, J. C.:
"Turbulent Boundary Layers with Pressure Gradients and Heat Transfer," Aerodynamische Versuchsanstalt, Goettingen, Bericht 64 A 26, July 1964

8. Rotta, J. C.:
"Heat Transfer and Temperature Distribution in Turbulent Boundary Layers at Supersonic and Hypersonic Flow," Recent Developments in Boundary Layer Research, AGARDograph 97, Part I, May 1965, pp. 35-63.

9. Rotta, J. C.:
"Recent Developments in Calculation Methods for Turbulent Boundary Layers with Pressure Gradients and Heat Transfer," Transactions of the ASME, Journal of Applied Mechanics, June 1966, pp. 429-437

REFERENCES (cont.)

10. Baronti, P.O. and Libby, P.A.:
"Velocity Profiles in Turbulent Compressible Boundary Layers," AIAA Journal, Vol. 4, No. 2, February 1966, pp. 193-202.

11. Coles, D.E.:
"The Turbulent Boundary Layer in a Compressible Fluid," RAND Corp. Report R-403-PR, September 1962.

12. Crocco, L.:
"Transformation of the Compressible Turbulent Boundary Layer with Heat Exchange," AIAA Journal, Vol. 1, No. 12, 1963, pp. 2723-2731.

13. Libby, P.A., Baronti, P.O. and Napolitano, L.:
"Study of the Incompressible Turbulent Boundary Layer with Pressure Gradient," AIAA Journal, Vol. 2, No. 3, March 1964, pp. 445-452.

14. Deissler, R.G. and Loeffler, A.L., Jr.:
"Analysis of Turbulent Flow and Heat Transfer on a Flat Plate at High Mach Numbers with Variable Fluid Properties," NASA TR-R-17, 1959.

15. Lin, C.C.:
Turbulent Flows and Heat Transfer, Vol. V, High Speed Aerodynamics and Jet Propulsion, Princeton University Press, Princeton, New York, 1959.

16. Spalding, D.B. and Chi, S.W.:
"The Drag of a Compressible Turbulent Boundary Layer on a Smooth Flat Plate With and Without Heat Transfer," Journal of Fluid Mechanics, Vol. 18, Part I, January 1964, pp. 117-143.

17. Cohen, N.B.:
"A Method for Computing Turbulent Heat Transfer in the Presence of a Streamwise Pressure Gradient for Bodies in High-Speed Flow," NASA Memo 1-2-59L, March 1959.

TABLE I

TEST CONDITIONS FOR NOZZLE WALL BOUNDARY LAYER EXPERIMENTS

SHOCK TUNNEL	CONDITION	SYMBOL	RUN	T_o ~°R.	P_o ~PSIA	BASED ON MEAS. WALL STATIC PRESS. R_{e_∞}/FT	BASED ON MEAS. WALL STATIC PRESS. M_∞	BASED ON NOZZLE PITOT PRESS. CALIB. R_{e_∞}/FT	BASED ON NOZZLE PITOT PRESS. CALIB. M_∞	δ~	δ^*~	θ~
CAL HST	2	○	3	1779	1004	2.88×10^6	1.62	2.74×10^6	7.76	2.0	.937	.060
48 INCH	↓	□	4	1820	1016	2.79	1.63	2.68	7.75	↓	↓	↓
LEG - NSR	1	○	5	1848	4233	11.3	7.87	10.89	7.97	1.77	.792	.050
33-009-029	↓	◇	6	1860	4242	11.1	7.89	10.79	7.97	↓	↓	↓
	3	◁	7	5741	986	0.28	7.27	0.37	6.64	2.54	1.20	.112
	↓	◇	8	5768	1003	0.27	7.35	0.37	6.62	↓	↓	↓
	2	△	9*	1808	974	2.60	7.75	2.60	7.75	2.0	.937	.060
	↓	◁	11	1859	1011	2.70	7.61	2.58	7.74	↓	↓	↓
	1	□	12	1831	4103	11.5	7.77	10.71	7.96	1.77	.792	.050
	↓	○	13	1776	4247	11.8	7.94	11.65	7.98	↓	↓	↓
	2	△	14	1909	1102	2.86	7.57	2.68	7.75	2.0	.937	.060
	3	▽	15	5680	1001	0.33	7.00	0.38	6.64	2.54	1.20	.112
	↓	○	16	5765	992	0.31	7.03	0.37	6.60	↓	↓	↓
CAL HST 96 INCH	4	◇	2	5031	921	0.38	7.21	0.44	6.85	2.73	1.21	.109
LEG (EX-	↓	○	3	5006	929	0.39	7.22	0.45	6.85	↓	↓	↓
PLORATORY	↓	○	4	5033	1014	0.38	7.21	0.44	6.84	↓	↓	↓
RUNS)												

*POOR STATIC PRESSURE DATA, FREESTREAM CONDITIONS COMPUTED FROM 1-D LE CALIBRATION

FIGURE 1

NOZZLE WALL BOUNDARY LAYER
PITOT PRESSURE PROFILES

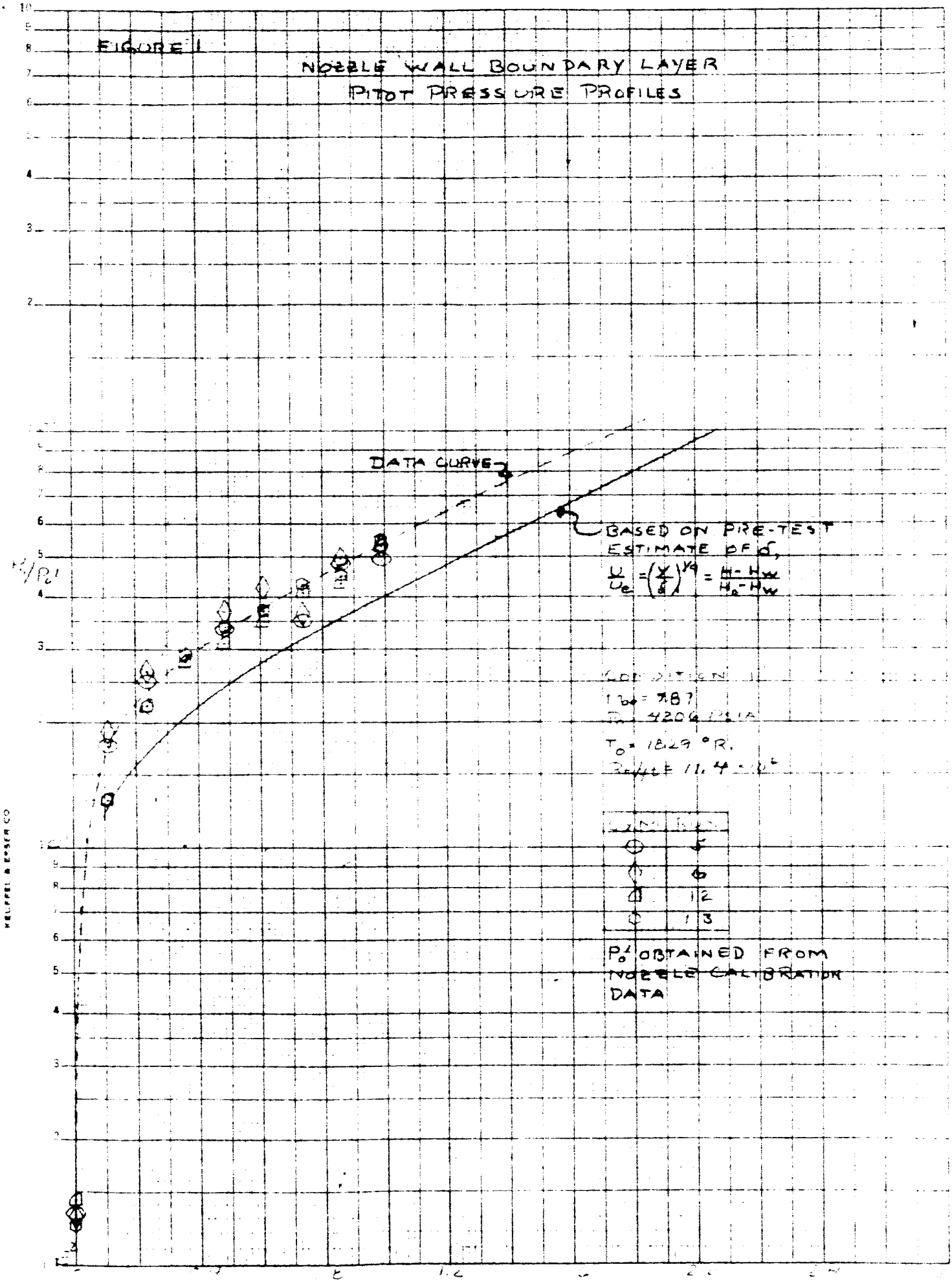

FIGURE 7 (CONTINUED)

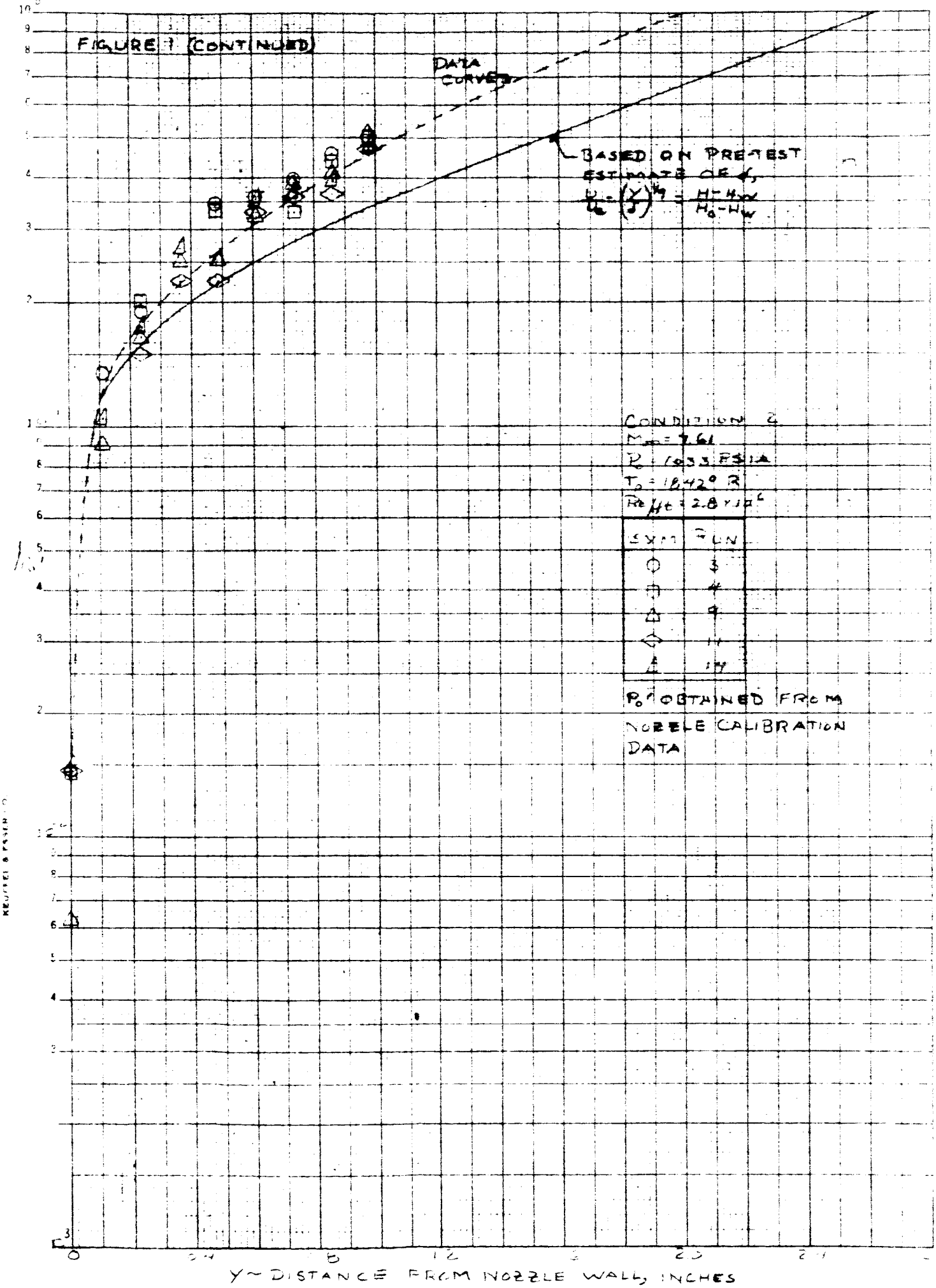

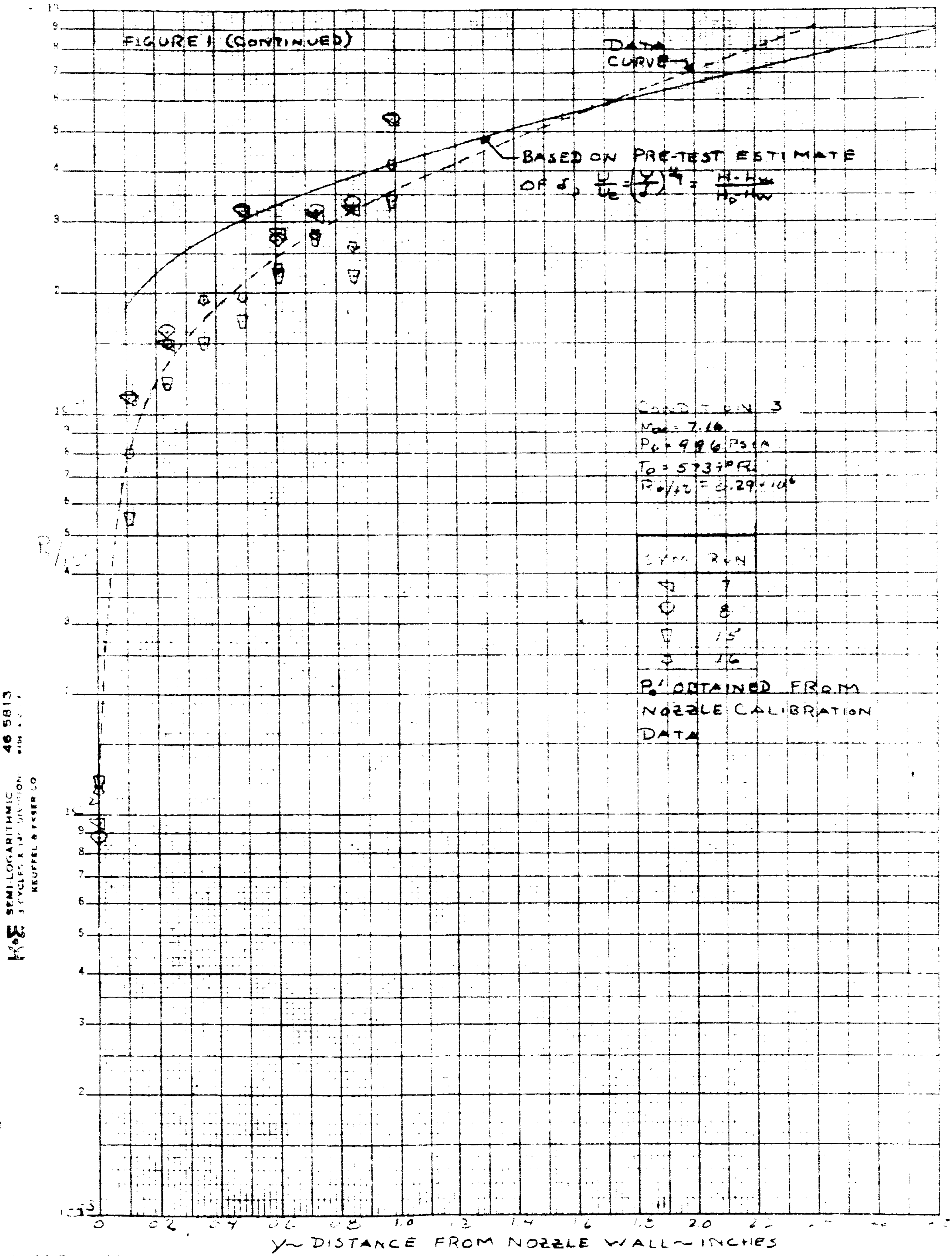
FIGURE 1 (CONTINUED)
DATA CURVE
BASED ON PRE-TEST ESTIMATE OF δ, U/Ue = (Y/δ)^1/4 = (H - Hw)/(Ho - Hw)
CONDITION 3
M∞ = 7.16
Po = 996 PSIA
To = 573?°R
SYM RUN
7
8
15
16
Po' OBTAINED FROM NOZZLE CALIBRATION DATA
0
0.2
0.4
0.6
0.8
1.0
1.2
1.4
1.6
1.8
2.0
2.2
Y ~ DISTANCE FROM NOZZLE WALL ~ INCHES
46 5813
SEMI-LOGARITHMIC
KEUFFEL & ESSER CO.

FIGURE 1 (CONTINUED)

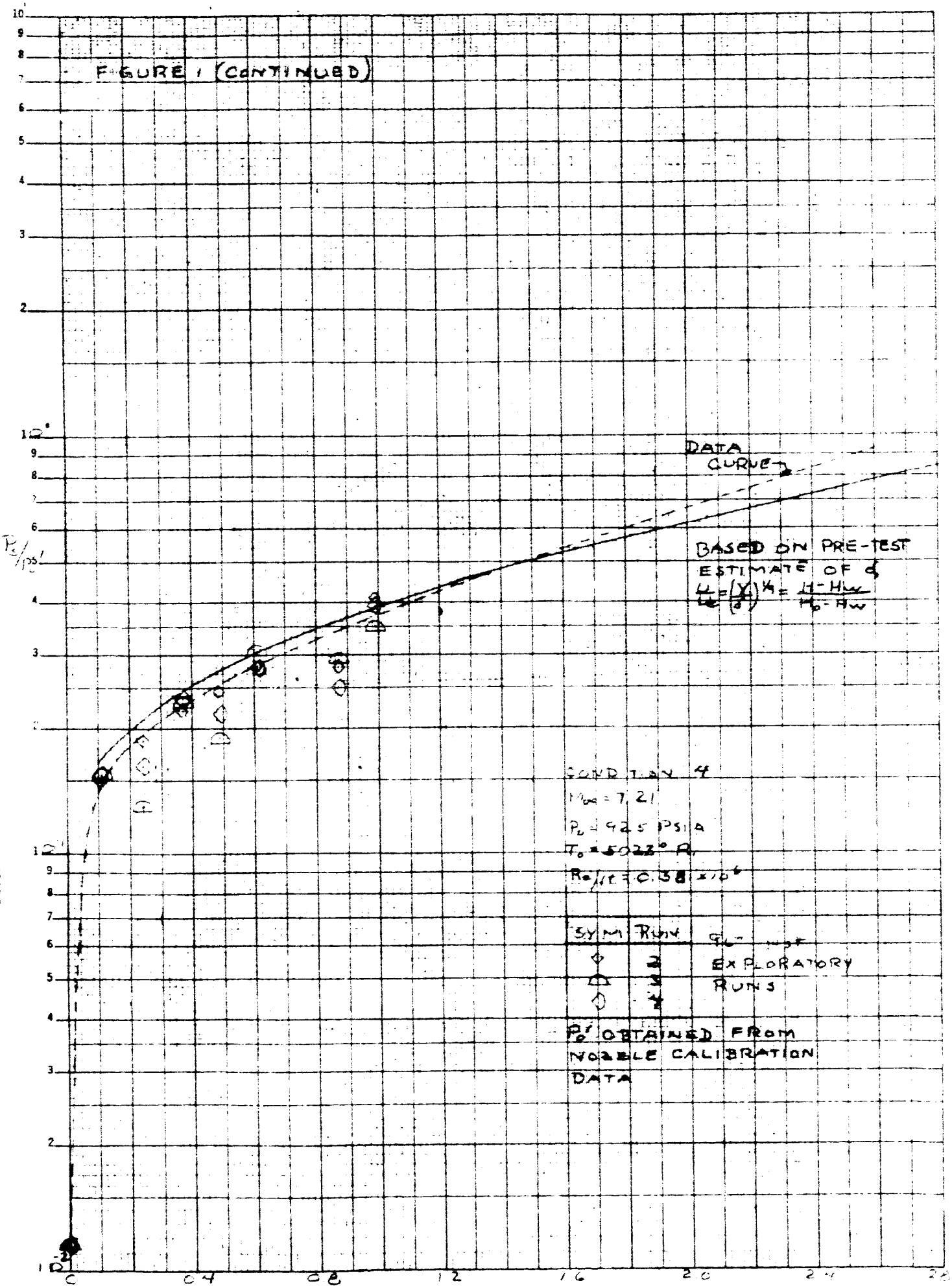

K&E SEMI-LOGARITHMIC 358-73

FIGURE 2 NOZZLE WALL BOUNDARY LAYER MACH NUMBER PROFILES

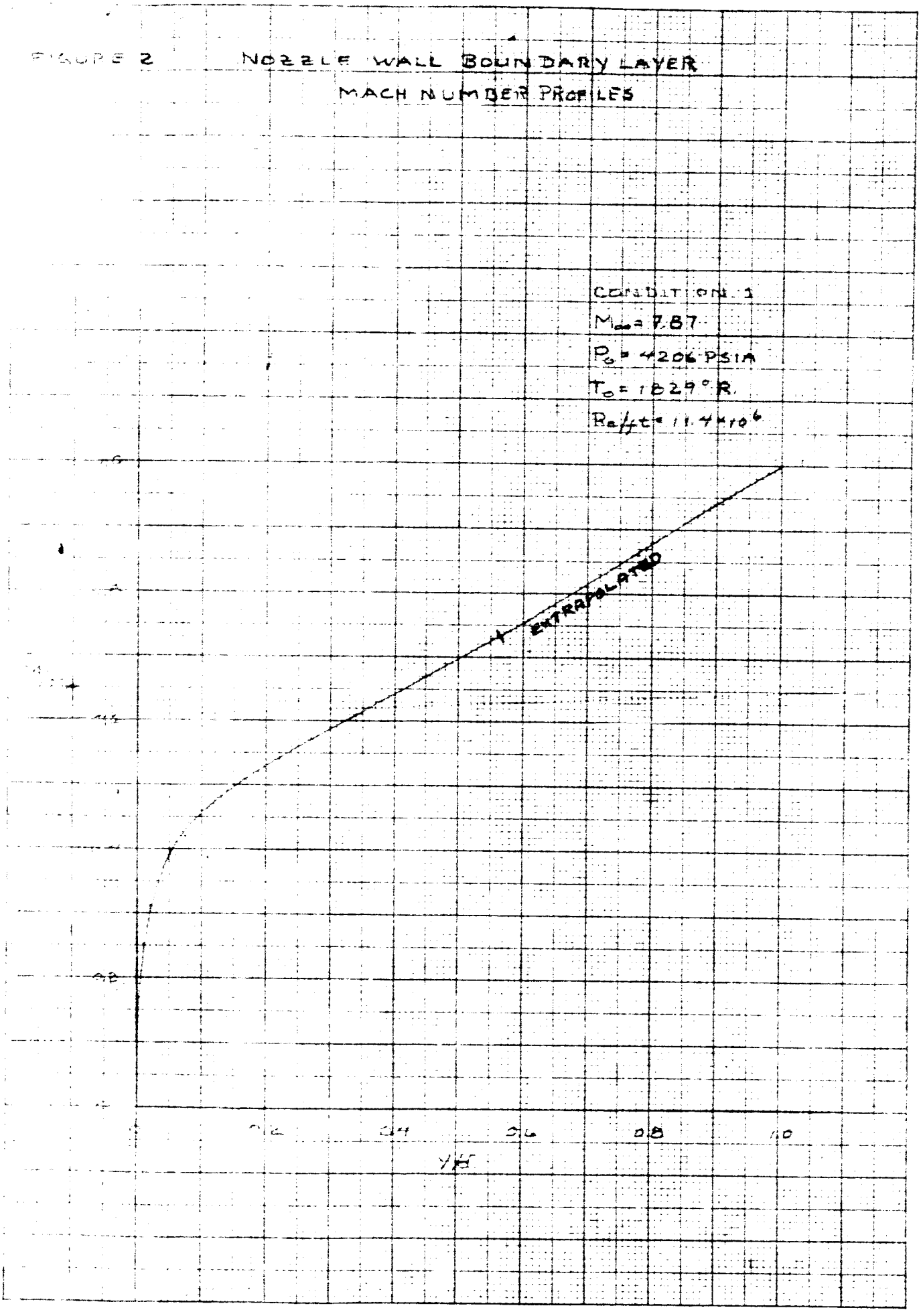

FIGURE 2 (CONTINUED)

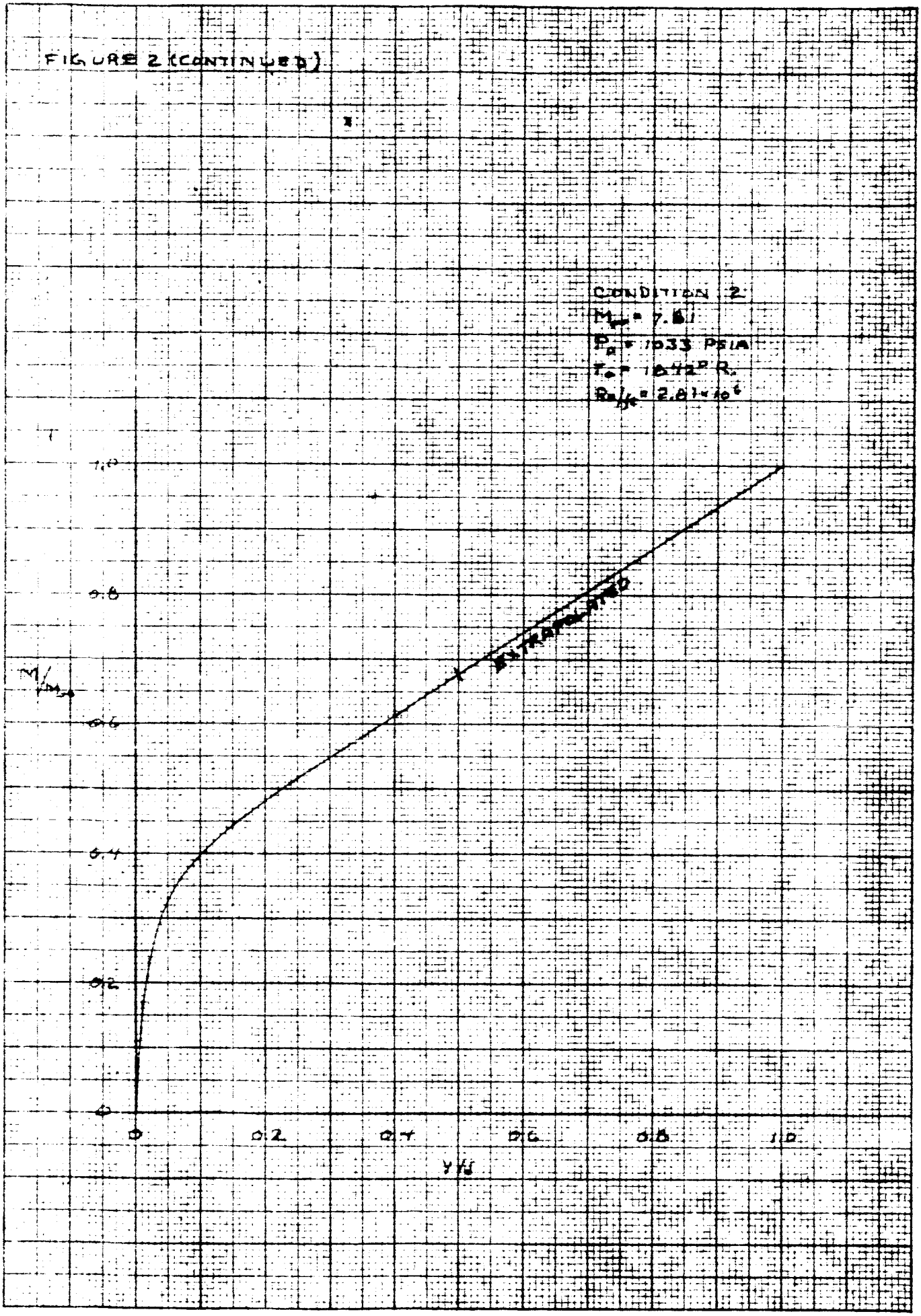

FIGURE 2 (CONTINUED)

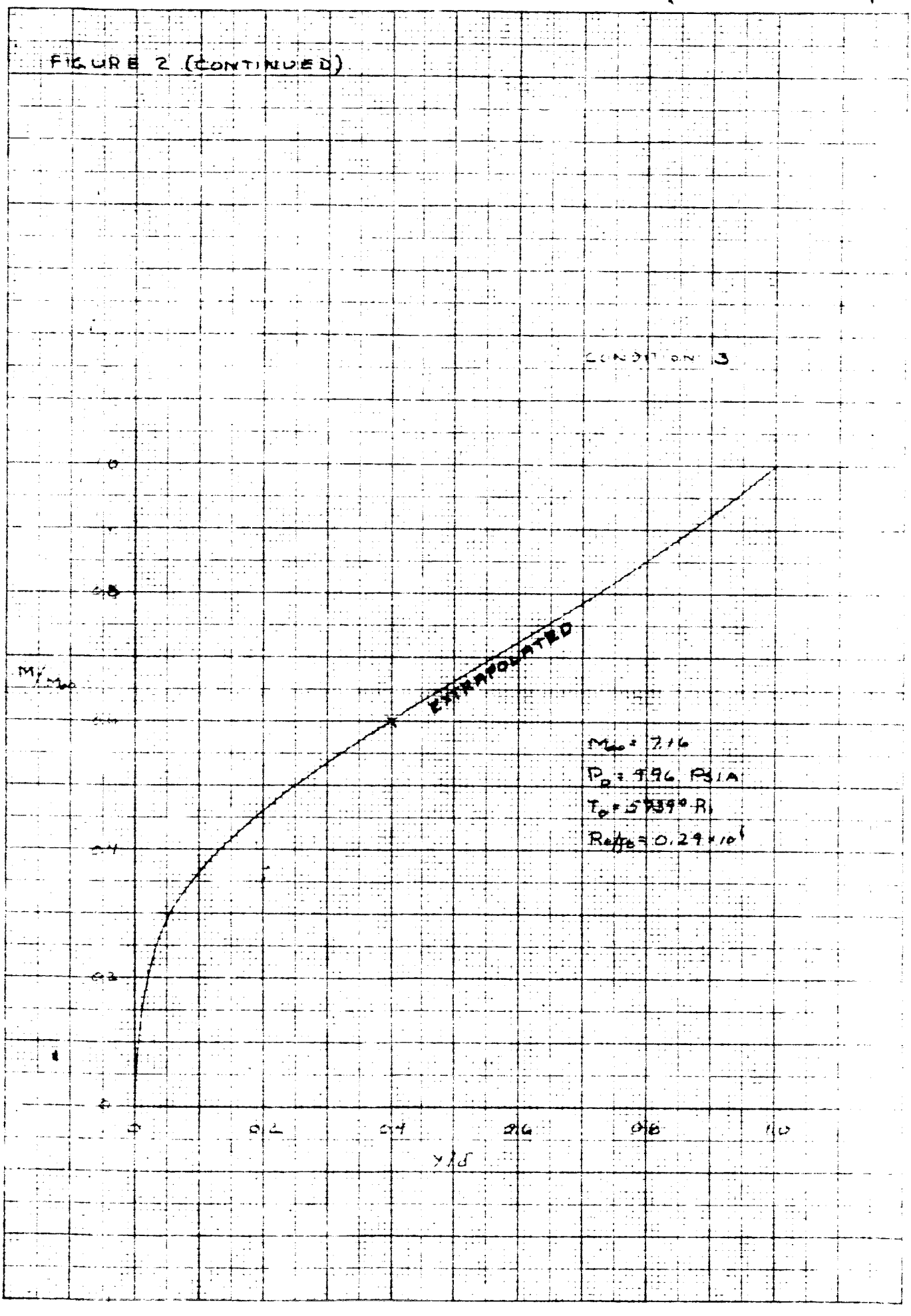

FIGURE 2 (CONTINUED)

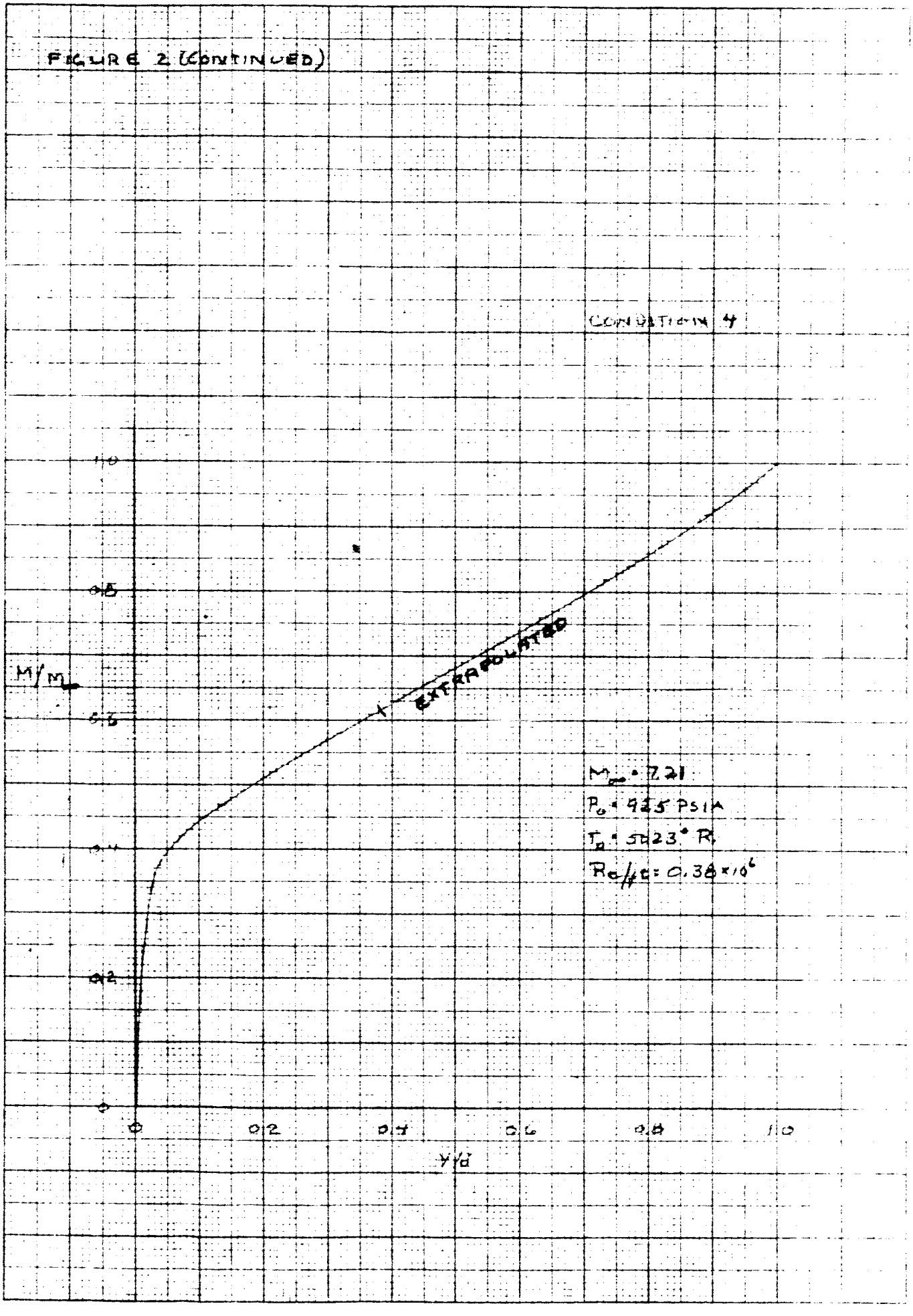

FIGURE 3 NOZZLE WALL BOUNDARY LAYER VELOCITY PROFILES

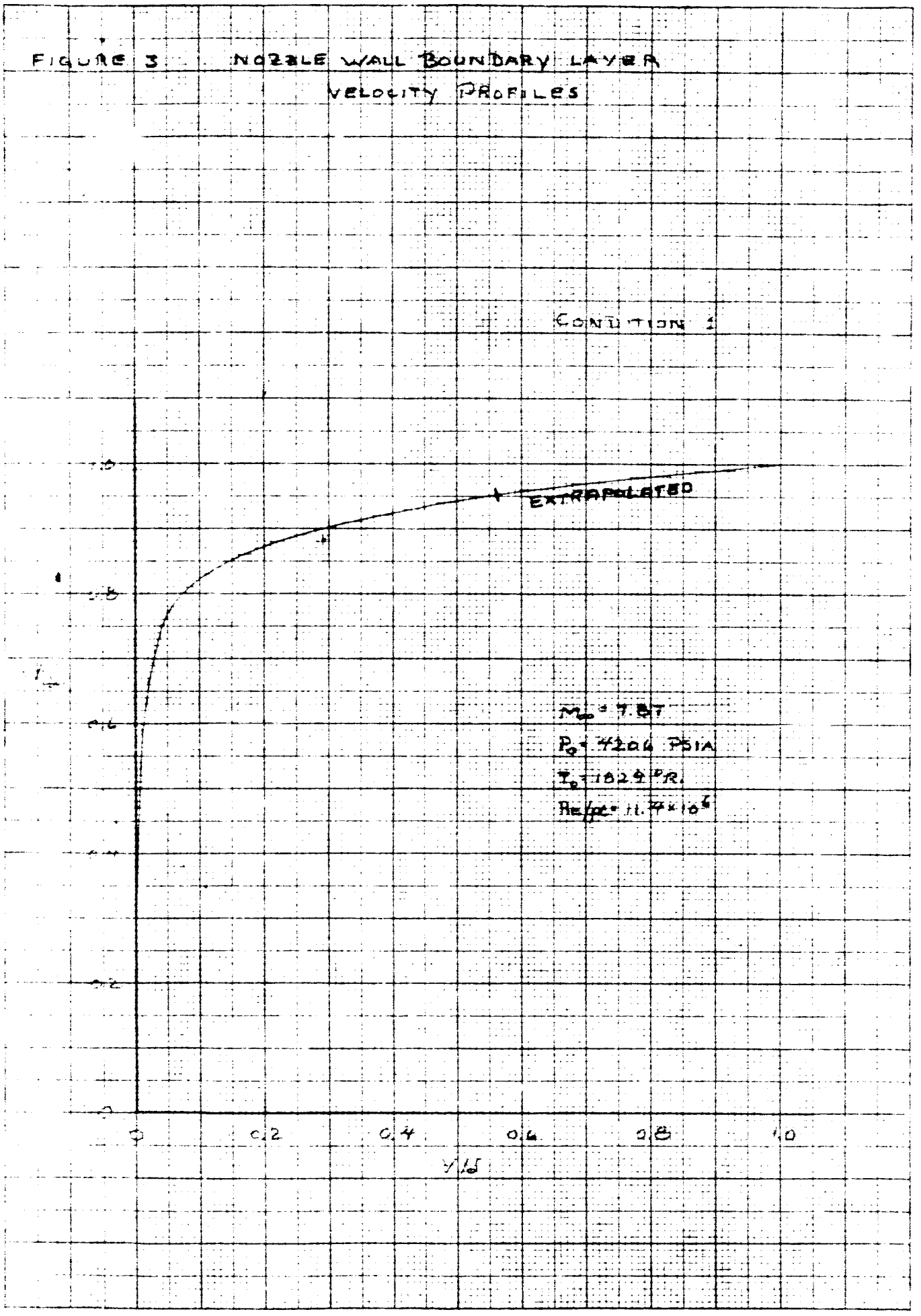

FIGURE 3 (CONTINUED)

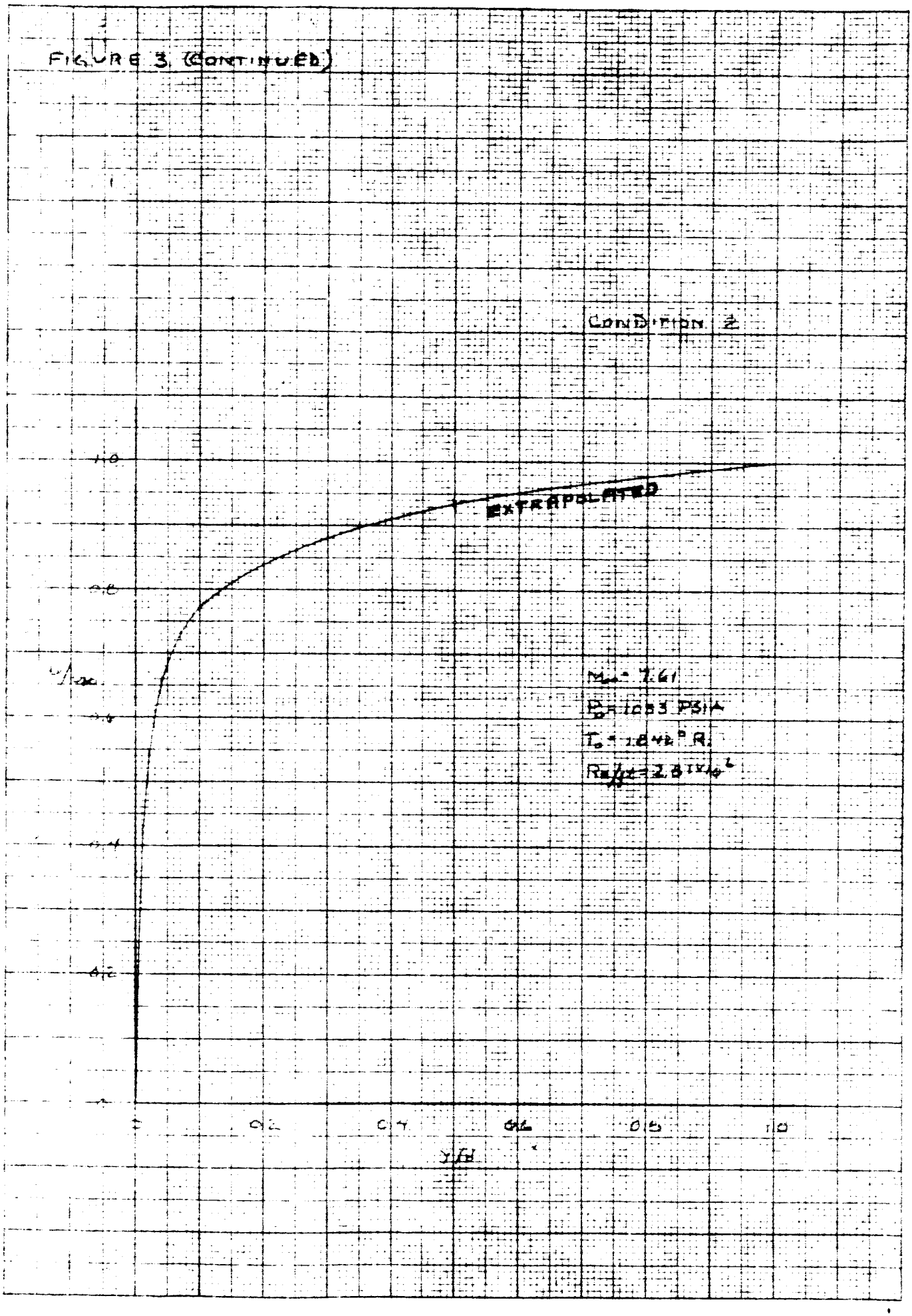

FIGURE 3 (CONTINUED)

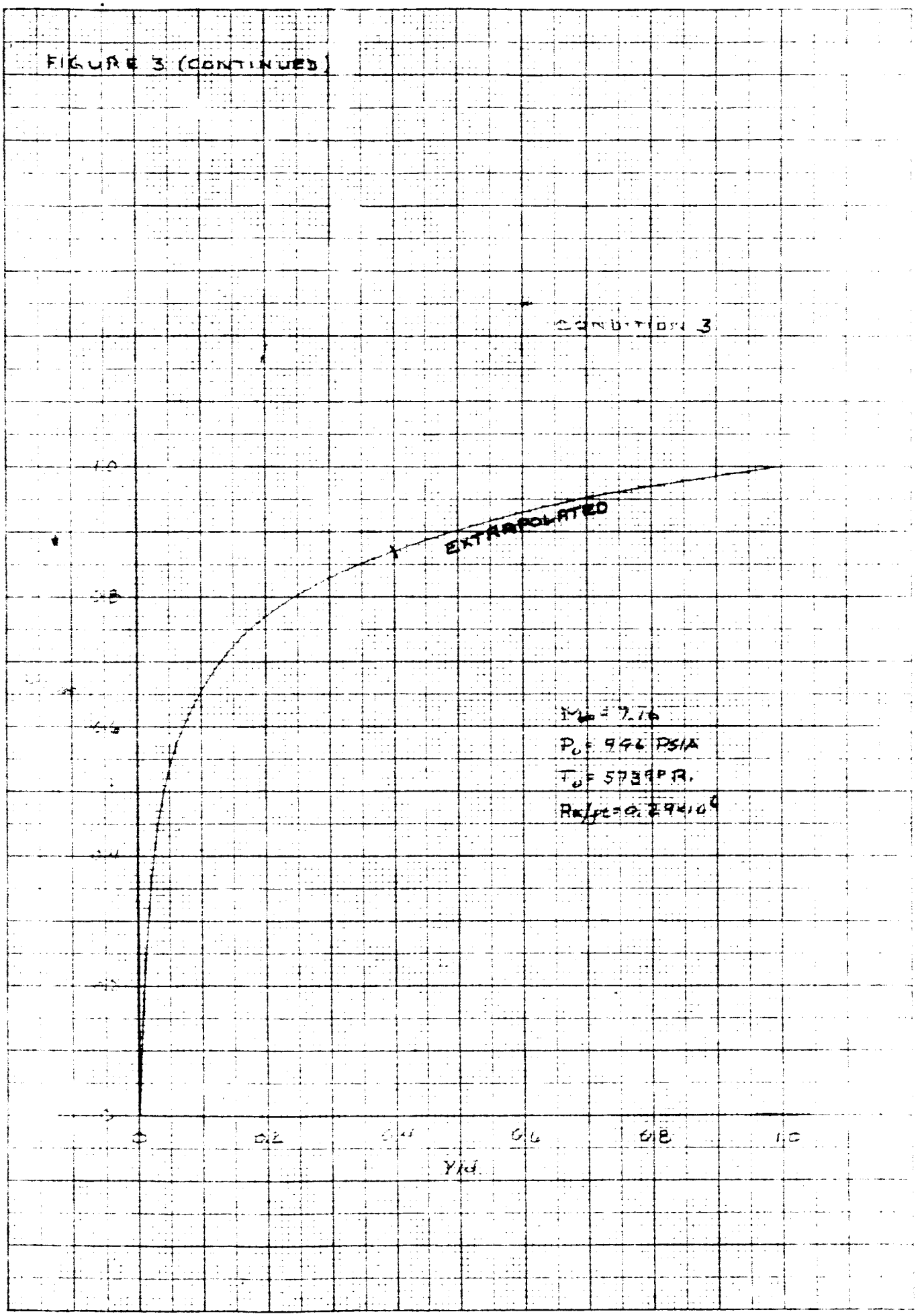

FIGURE 3 (CONTINUED)

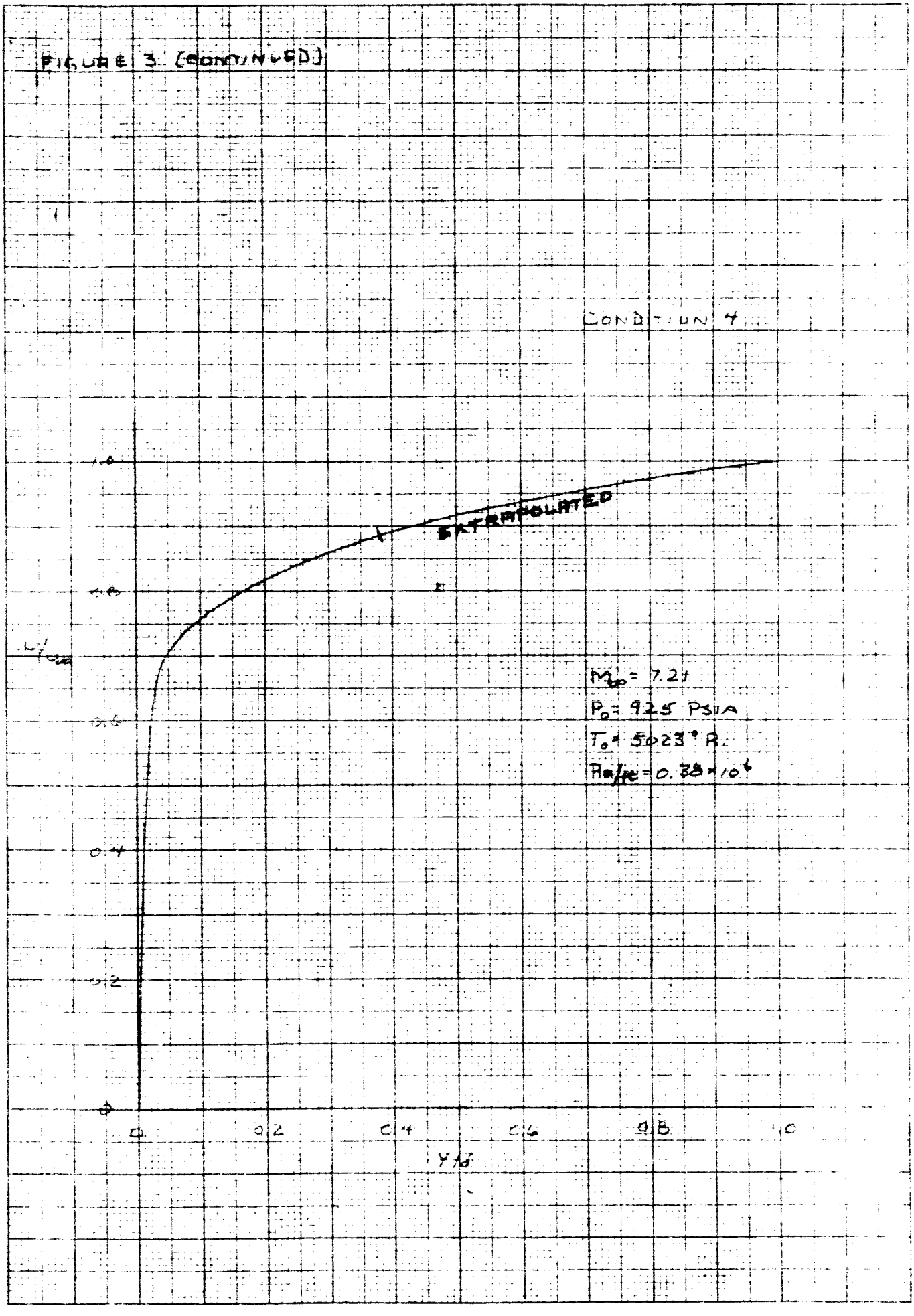

FIGURE 6 - NOZZLE WALL SKIN FRICTION COEFFICIENT VS. MOMENTUM THICKNESS REYNOLDS NUMBER

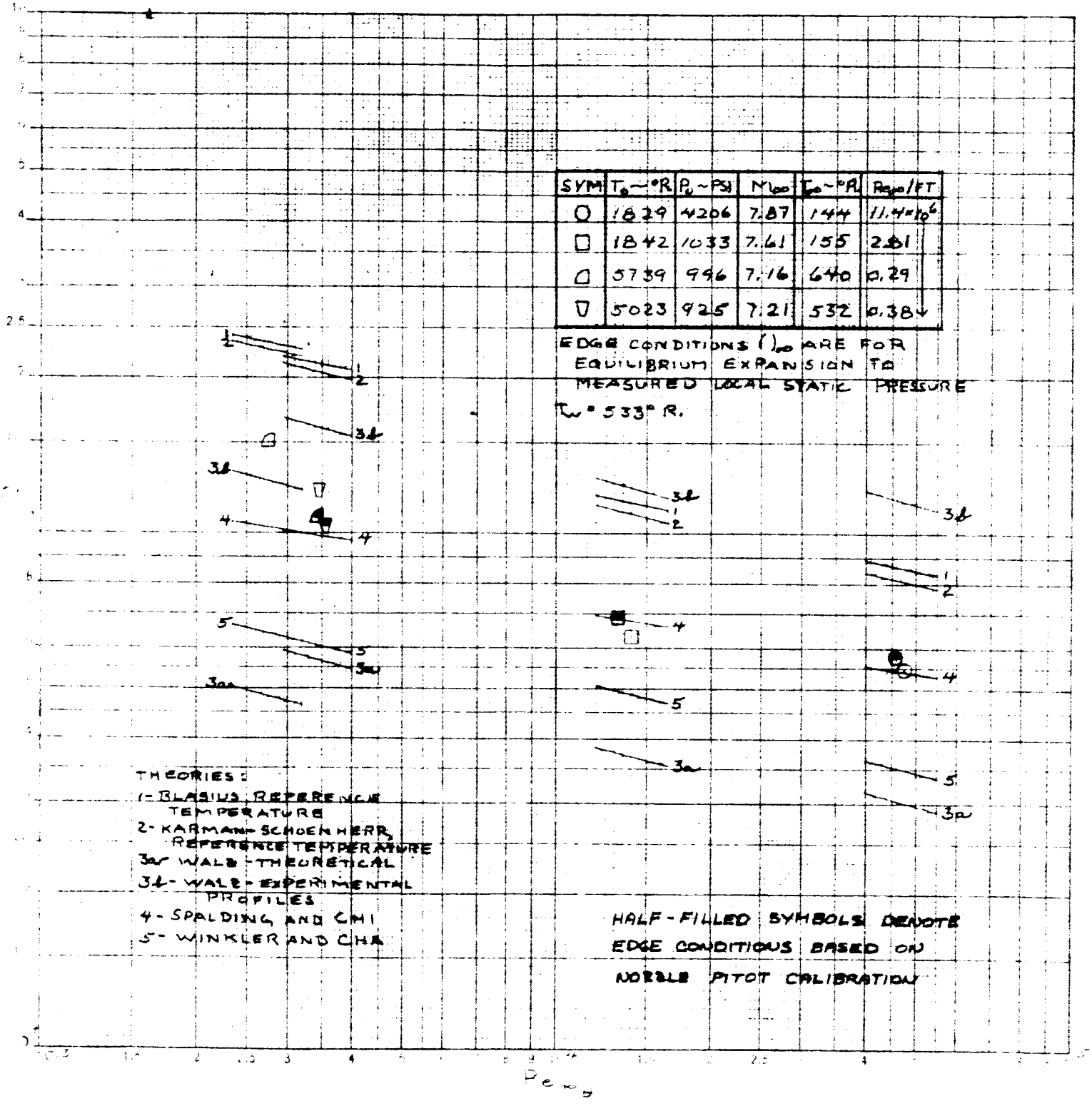

FIGURE 7 NOZZLE WALL STANTON NUMBER VS. MOMENTUM THICKNESS REYNOLDS NUMBER

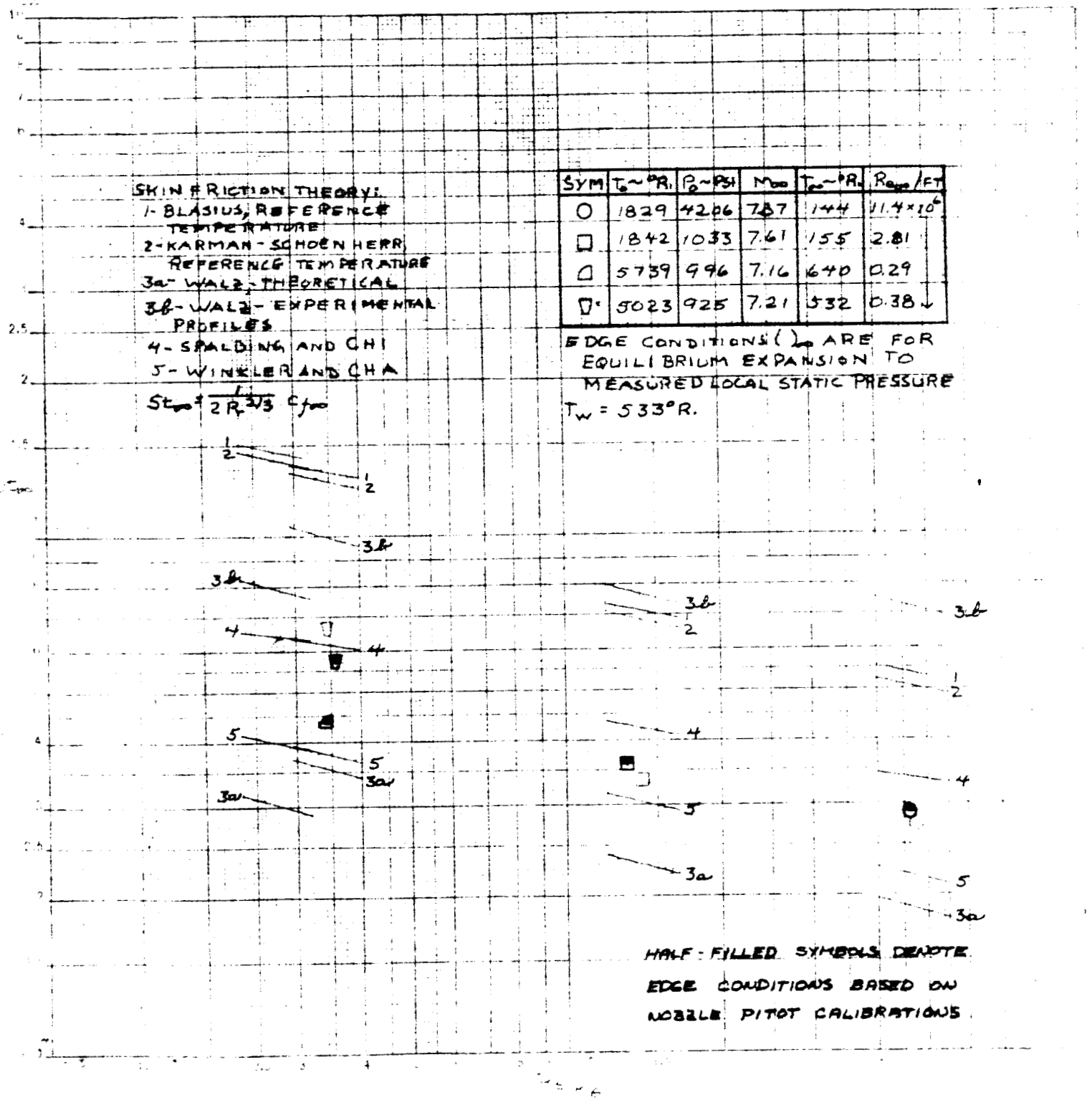

FIGURE 8 SPALDING-CHI SKIN FRICTION CORRELATION

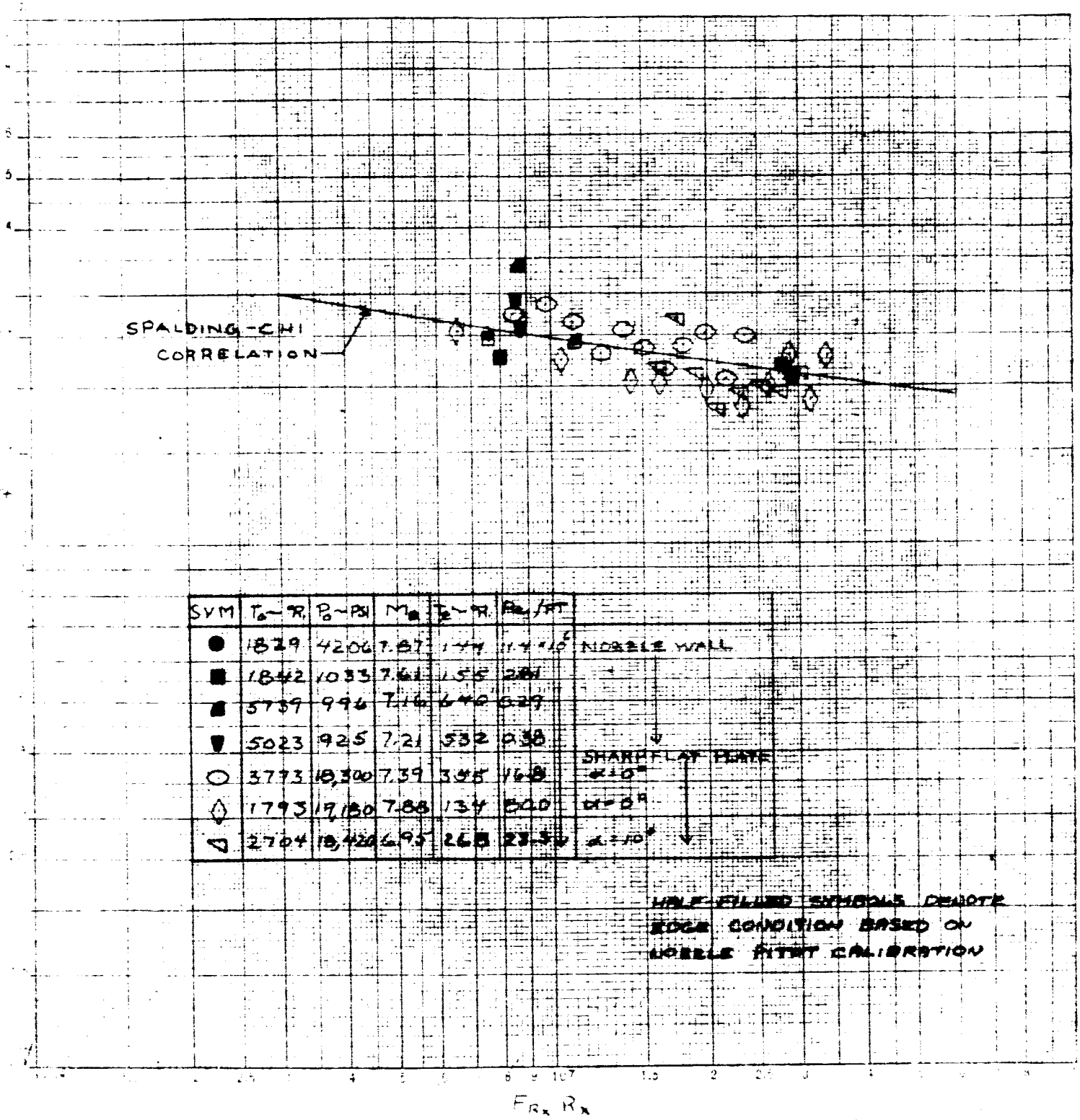

SYM	T_o~°R	P_o~PSI	M_e	T_e~°R	Re_e/FT
●	1829	4206	7.87	1144	11.4×10^6
■	1842	1033	7.61	155	2.81
■	5739	996	7.16	646	6.27
▼	5023	925	7.21	532	9.38
○	3773	18,300	7.39	395	16.8
◇	1793	17,180	7.88	134	50.0
◁	2704	18,420	6.95	268	23.3

FIGURE 9

SPALDING-CHI STANTON NUMBER CORRELATION

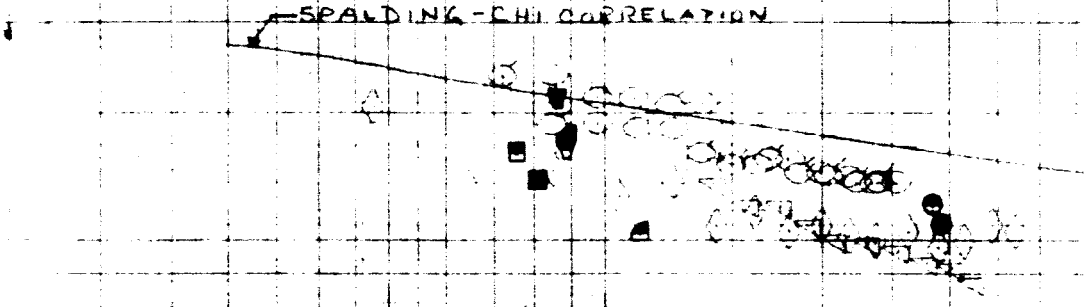

SYM	T_o~PR.	P_o~PSI	M_e	T_e~PR.	R_e/ft	
●	1829	4206	7.87	144	11.4×10^6	NOZZLE WALL
■	1842	1083	7.61	155	2.81	
▲	5739	996	7.16	640	0.28	
▼	5023	925	7.21	532	0.38	
○	3773	18,300	7.39	355	16.8	SHARP FLAT PLATE $\alpha=0°$
◇	1793	19,180	7.86	134	800	$\alpha=0°$
◁	2704	43,420	6.95	268	233	$\alpha=10°$

FLAGGED SYMBOLS - CORRECTED FOR VIRTUAL ORIGIN

HALF-FILLED SYMBOLS DENOTE EDGE CONDITIONS BASED ON NOZZLE PITOT CALIBRATION